Eur. Phys. J. A **13**, 87–92 (2002)

THE EUROPEAN PHYSICAL JOURNAL A

Decoupling and coherence in E1 and E2 moments in drip line nuclei

H. Sagawa

Center for Mathematical Sciences, University of Aizu, Aizu-Wakamatsu, Fukushima 965-8580, Japan

Received: 1 May 2001

Abstract. I discuss first the effect of decoupling of extended wave functions and the coherence in the low-energy $E1$ strength in drip line nuclei ^{12}Be and ^{13}O, which are studied by large-scale shell model calculations including $3\hbar\omega$ configuration space. The calculated results are compared to recent experimental data of Coulomb excitations. The quenching of the core polarization charges in drip line nuclei is also discussed in relation to recent observations of quadrupole moments in B-isotopes.

PACS. 21.10.Ky Electromagnetic moments – 21.60.Jz Hartree-Fock and random-phase approximations – 23.20.-g Electromagnetic transitions

1 Introduction

Neutron and proton drip line nuclei have been studied intensively because of its interesting exotic structure due to the loose binding of valence neutrons and protons [1]. Much attention is paid now on electric dipole ($E1$) excitations in very low-energy region of the nucleus with loosely bound nucleons [2–8]. The $E1$ strength in stable nuclei is largely exhausted by giant dipole resonance (GDR), which is considered as a collective vibration mode constructed from a coherent superposition of particle-hole excitations crossing one major shell. The experimental excitation energy of GDR is found at $E_x = 80/A^{1/3}$ MeV, exhausting most of the sum rule strength, while the $E1$ strength in low-energy region below 5 MeV is observed to be negligibly small in stable nuclei. On the other hand, abnormally large $E1$ strength is confirmed experimentally in some light unstable nuclei in the low-energy region below 5 MeV. The transition between the ground state with $J^\pi = \frac{1}{2}^+$ and the first excited $\frac{1}{2}^-$ state at $E_x = 0.32$ MeV in $^{11}_4$Be$_7$ is a well-known example of this anomaly, representing the strongest $E1$ transition ever observed between bound states [2]. A strong $E1$ transition to the bound 1^- state at $E_x = 2.68$ MeV is also found in $^{12}_4$Be$_8$ very recently [3]. Such strong $E1$ transitions may indicate a decoupled feature between the excitations of extended loosely bound states and those of the core configurations [4]. The measurements of the low-lying $E1$ strength have been extended to the continuum excitations of neutron-rich nuclei $^{11}_3$Li$_8$ [5–7] and $^{11}_4$Be$_7$ [8], where the loosely bound "halo" neutrons play an essential role to increase the strength.

Recently, the possible shell melting is often discussed in nuclei near drip lines, especially in relation with the magic numbers 8 and 20 [3,9–11]. Evidence of disappearance of magicity $N = 8$ in $^{12}_4$Be$_8$ has been claimed recently from the study of proton inelastic scatterings [11] and Coulomb excitations on $^{12}_4$Be$_8$ [3]. The melting shell structure at the magic number 8 may be caused by much smaller energy gap between the p and sd shells than expected for the standard shell gap, *i.e.*, $\hbar\omega = 41/A^{1/3}$ MeV. The near degeneracy of $2s_{1/2}$ and $1p_{1/2}$ orbits relevant to the smaller energy gap may bring down a decoupled 1^- state at much lower energy than GDR energy region. Another possible effect of the shell melting is a strong correlation among the valence nucleons outside of the core, which may cause a coherent effect in the transition amplitudes and enhance the low-energy $E1$ strength largely. We study the $E1$ strength distributions of $^{12}_4$Be$_8$ and $^{13}_8$O$_5$ focusing on the problem of $N = 8$ magicity in sect. 2.

Recently, precise measurements of electric quadrupole moments (Q-moments) become possible in nuclei far from the stability line by the use of radioactive nuclear beams [12–14]. These data make it possible to study N/Z-dependence of the effective charges up to the ratio $N/Z \sim 2.54$. In nuclei far from stability, it is expected that the core polarization is weakly induced by particles with extended tail due to small binding energies and small orbital angular momentum ($\ell = 0$ or 1) [15,16]. This is because those particles spend an appreciable amount of time outside the core of nucleus and, thus, cannot efficiently polarize the core. This decoupling effect on the polarization charges has the same physical origin as the one for the low-energy $E1$ strength. In sect. 3, we study a quenching feature of core polarization charges in relation with the quadrupole moments of B-isotopes near the stability line to the neutron drip line. This paper is organized as

follows. Section 2 is devoted to the study of $E1$ strength in $^{12}_{4}\mathrm{Be}_8$ and $^{13}_{8}\mathrm{O}_5$. The core polarizations and Q-moments are discussed in sect. 3. A summary is given in sect. 4.

2 Low-energy E1 transitions in drip line nuclei

We study the $E1$ strength distributions of two nuclei $^{12}_{4}\mathrm{Be}_8$ and $^{13}_{8}\mathrm{O}_5$ focusing on the problem of $N = 8$ magicity [17]. As the theoretical framework, we adopt a large-scale shell model including $(0 + 2)\hbar\omega$ model space for the ground states and $(1 + 3)\hbar\omega$ model space for the excited states. The shell model calculations are performed by using the program OXBASH [18]. Millener-Kurath interaction PSDMK2 [19] and Warburton-Brown interaction WBP [20] are used as the effective interactions for the ($1p$-$2s1d$) model space and for ($1s$-$1p$-$2s1d$-$1f2p$) model space, respectively. For PSDMK2 interaction, the single-particle energy of the $2s_{1/2}$ orbit is lowered to admix sd shell components largely in the ground state as suggested by recent analysis of spectroscopic factor measurements [9]. We name this interaction PSDMK2*. We use the effective $E1$ transition operator

$$\hat{O}^{\lambda=1}_{\mu} = e\frac{Z}{A}\sum_{i}^{N} r_i Y_{1\mu}(\hat{r_i}) - e\frac{N}{A}\sum_{i}^{Z} r_i Y_{1\mu}(\hat{r_i}) \qquad (1)$$

in which the spurious center-of-mass motion is subtracted from the isovector dipole transition operator. The $E1$ transition strength to n-th excited state at energy E_n is defined as

$$B(E1, E_n) = \frac{1}{2J_i+1}\sum_{M_i,\mu,M_f} |\langle n; J_f, M_f \mid \hat{O}^{\lambda=1}_{\mu} \mid J_i, M_i\rangle|^2 . \qquad (2)$$

The transition strength is averaged by a weight factor $\rho(E)$ as

$$\frac{\mathrm{d}B(E1;Ex)}{\mathrm{d}Ex} = \sum_{n} B(E1;E_n)\rho(Ex - E_n) , \qquad (3)$$

where

$$\rho(Ex - E_n) = \frac{1}{\pi}\frac{\Gamma/2}{(Ex - E_n)^2 + (\Gamma/2)^2}. \qquad (4)$$

The weight factor can be considered to simulate the escape and the spreading widths.

In fig. 1(a), we show two calculated results of the dipole transitions in $^{12}_{4}\mathrm{Be}_8$ by PSDMK2* with the extended single-particle wave functions and with the harmonic-oscillator wave functions. We can see from fig. 1(a) that substantial strength appears at $E_x = 2.36$ MeV far below the GDR region at $E_x = 10$–13 MeV, only when the effect of the extended single-particle wave functions is switched on. On the other hand, the GDR peaks found above $E_x = 10$ MeV are not so much affected by the effect of the extended single-particle wave functions. The low-energy transition strength is found to be $B(E1) = 0.063e^2\,\mathrm{fm}^2$ at $E_x = 2.36$ MeV. This $B(E1)$ value corresponds to 0.19 Weisskopf unit (W.u.) and amounts to 0.4% of the TRK sum rule value and 4.0% of the cluster sum rule value. The calculated value shows good agreement with the observed value $B(E1) = 0.051(13)e^2\,\mathrm{fm}^2$ at $E_x = 2.68(3)$ MeV by recent Coulomb excitation experiments [3]. This $E1$ strength corresponds to the second largest $E1$ strength among the transitions between bound states, next to the largest transition $B(E1) = 0.36 \pm 0.03$ W.u. between $1/2^+$ and $1/2^-$ states in $^{11}_{4}\mathrm{Be}_7$. We have done also more elaborate shell model calculations including the $1f2p$ shell configurations in addition to the $1p$-$2s1d$ shells with WBP interaction and found very similar results to those of PSDMK2* as far as the low-energy strength is concerned.

The large $E1$ strength in the very low-energy region below $E_x = 3$ MeV might involve a coherence in the oscillation between the loosely bound neutrons, and also between the core and the loosely bound neutrons. The ground state of $^{12}_{4}\mathrm{Be}_8$ is considered as a state of correlated two neutrons in $(1p_{1/2})^2$, $(2s_{1/2})^2$ and $(1d_{5/2})^2$ states moving outside the ^{10}Be core,

$$|^{12}_{4}\mathrm{Be}_8 : 0^+\rangle = \alpha|(1p_{1/2})^2\rangle + \beta|(2s_{1/2})^2\rangle + \gamma|(1d_{5/2})^2\rangle. \quad (5)$$

In order to illustrate the mechanism of the enhancement due to the halo configurations, we take a simplified pair configuration of $(1p_{1/2})^2$ and $(2s_{1/2})^2$ states for the ground state of $^{12}_{4}\mathrm{Be}_8$, although the $(1d_{5/2})^2$ configuration may have a substantial occupation probability [9]. In the limit of the complete degeneracy of the two orbitals, we have the amplitudes $\alpha = \beta = \frac{1}{\sqrt{2}}$. Then a coherent 1^- excitation of the correlated two neutrons is written as a doorway state for the dipole operator (1),

$$|^{12}_{4}\mathrm{Be}_8 : 1^-\rangle = \frac{1}{\sqrt{N}}\hat{O}^{\lambda=1}|^{12}_{4}\mathrm{Be}_8 : 0^+\rangle = 0.63|(2s_{1/2}1p^{-1}_{1/2})\rangle + 0.63|(1p_{1/2}2s^{-1}_{1/2})\rangle + 0.45|(2s_{1/2}1p^{-1}_{3/2})\rangle, \qquad (6)$$

where N is a normalization constant, and the coefficients are proportional to the single-particle matrix elements of the dipole operator $\hat{O}^{\lambda=1}$ [3,21]. In eq. (6), the particle-hole excitations are limited to the configuration space of $1p$ and $2s$ orbitals to pin down specifically the coherence in the loosely bound neutron configurations. The coefficients of the p-h configurations are obtained taking into account the effect of small separation energies of the $1p_{1/2}$ and $2s_{1/2}$ states in $^{12}_{4}\mathrm{Be}_8$. The $B(E1)$ value between the two states (5) and (6) is expressed as

$$B(E1; 0^+ \to 1^-) = |\langle 1^-||\hat{O}^{\lambda=1}||0^+\rangle|^2 = |0.63\langle 2s_{1/2}||\hat{O}^{\lambda=1}||1p_{1/2}\rangle + 0.63\langle 1p_{1/2}||\hat{O}^{\lambda=1}||2s_{1/2}\rangle + 0.45\langle 2s_{1/2}||\hat{O}^{\lambda=1}||1p_{3/2}\rangle|^2. \qquad (7)$$

We can see in eq. (7) that the degeneracy of $1p_{1/2}$ and $2s_{1/2}$ states indeed enhances the $B(E1)$ value more than

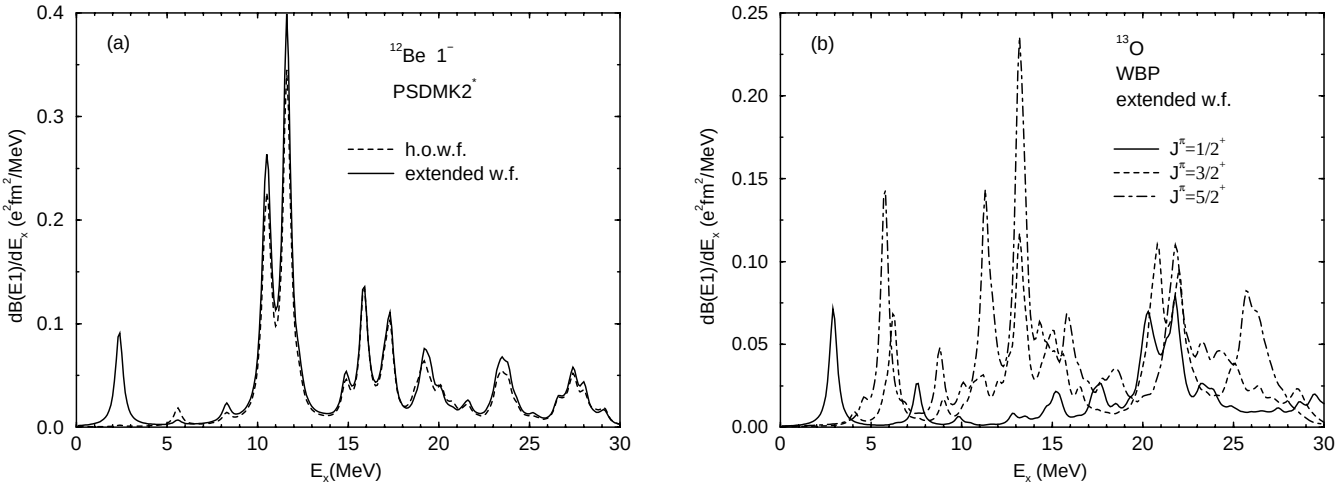

Fig. 1. (a) Calculated results of $E1$ strength distribution in $^{12}_{4}\mathrm{Be}_8$. The solid curve shows the result with the effect of the extended single-particle wave functions , while the dashed one corresponds to that with the harmonic-oscillator wave functions: with PSDMK2* interaction. (b) Calculated results of $E1$ strength distribution in $^{13}_{8}\mathrm{O}_5$ with WBP interaction. The solid, dashed and dot-dashed curves show the $E1$ strength to $J^\pi = 1/2^+$, $3/2^+$ and $5/2^+$ states, respectively, with the effect of the extended single-particle wave functions.

twice of the single-particle transition rate between $1p_{1/2}$ and $2s_{1/2}$ states. It should be noticed that the configurations associated with $1d_{5/2}$ state have also significant contributions to the $E1$ transition amplitude in the present shell model results. Especially, the $(1p_{3/2} \rightarrow 1d_{5/2})$ excitation has a substantial effect together with the configurations of eq. (7).

Recently, the spectroscopic factor measurements were performed in the one-neutron knockout reaction of $^{12}_{4}\mathrm{Be}_8$ [9]. The resulting spectroscopic factors suggest that two-thirds of the last neutron pairs occupies the $(2s\text{-}1d)^2$ shell configurations although direct measurement of $1d$ spectroscopic factors is still missing. The calculated occupation probabilities of the paired neutrons by PSDMK2* are 34.2% for the $(1p)^8$ and 65.8% for $(1p)^6(2s,1d)^2$ configurations in the ground state of $^{12}_{4}\mathrm{Be}_8$, which is consistent with the current experimental information.

In fig. 1(b), the $E1$ strength from the ground state $J^\pi = 3/2^-$ to the excited states $J^\pi = 1/2^+$, $3/2^+$ and $5/2^+$ in $^{13}_{8}\mathrm{O}_5$ is drawn by the solid, dashed and dash-dotted curves, respectively, with the effect of the extended single-particle wave functions. The large low-energy strength in $^{13}_{8}\mathrm{O}_5$ appears mainly in the three states at $E_x = 2.92$ MeV $(1/2^+)$, 5.76 MeV $(5/2^+)$ and 6.25 MeV $(3/2^+)$ as shown in fig. 1(b). For the three states, the proton particle-hole transitions, $(\pi 1p_{1/2} \rightarrow \pi 2s_{1/2})$, $(\pi 2s_{1/2} \rightarrow \pi 1p_{1/2})$ and $(\pi 1p_{3/2} \rightarrow \pi 2s_{1/2})$ transitions, contribute coherently to enhance the strength. The former two configurations are due to the excitations of the center of mass of the two loosely bound configurations $(\pi 2s_{1/2})^2$ and $(\pi 1p_{1/2})^2$, while the last one is the excitation of the core particle to the loosely bound orbit. This microscopic structure of the wave functions suggests a coherent excitation between the loosely bound protons, and also between the core and the loosely bound protons, similar to the excitations in the nuclei with loosely bound neutrons $^{11}_{3}\mathrm{Li}_8$ and $^{12}_{4}\mathrm{Be}_8$. Then this coherent excitation couples with the neutron hole configuration $(\nu 1p_{3/2})^{-1}$ and splits the $B(E1)$ strength to the three low excited states, while the proton particle $(\pi 1p_{3/2})$ state couples with the neutron vibrational state in $^{11}_{3}\mathrm{Li}_8$ [21].

It is useful introduce the particle-vibration coupling model to understand the microscopic structure of the splitting of low-energy dipole excitations in $^{13}_{8}\mathrm{O}_5$. Since the three valence neutrons in the $1p_{3/2}$ shell can make only the configuration of seniority 1, it is convenient to adopt the hole picture, instead of the particle one which was adequate for $^{11}_{3}\mathrm{Li}_8$. The hole-vibration coupling gives the same intensity rule for the transition strength as that of the particle-vibration coupling, but the energy splitting will be changed in the opposite direction. The $B(E1)$ values for the coupled states are related to the $B(E1)$ value of the 1^--phonon excitation in the core as [22]

$$B(E1; 3/2^- \rightarrow (1^- \times 3/2^-)J) = \frac{2J+1}{3 \cdot 4} B(E1; 0^+ \rightarrow 1^-). \tag{8}$$

The particle-vibration coupling model can be also applied to calculate the energy splitting of the low-energy dipole states. Assuming an interaction of the separable form $(Y^{(2)} \times Y^{(2)})^{(0)}$ for the hole-phonon coupling, the energy shift of the low-energy dipole state with spin J is given by

$$\langle (1p_{3/2})^{-1} \times (1^-); J \mid H \mid (1p_{3/2})^{-1} \times (1^-); J \rangle = \omega_{1^-} + \begin{cases} -5c_2, & \text{for } J = 1/2^+ \\ 4c_2, & \text{for } J = 3/2^+ \\ -c_2, & \text{for } J = 5/2^+ \end{cases}, \tag{9}$$

Table 1. Static IS and IV core polarization charges calculated for neutron and proton orbitals in ^{12}C by using SIII force. The $e_{\rm pol}$(IS) and $e_{\rm pol}$(IV) values are obtained by using eqs. (11) and (12) with $\varepsilon_i - \varepsilon_j = 0$. The $B(\lambda=2)_{\rm sp}$ value for the transition from the state $\mid i\rangle$ to $\mid f\rangle$ is calculated with the charges $e_n = e_p = 1$ for each configuration using the HF wave functions.

States		Neutrons			Protons		
f	i	$B(\lambda=2)_{\rm sp}$ (fm^4)	$e_{\rm pol}$(IS)	$e_{\rm pol}$(IV)	$B(\lambda=2)_{\rm sp}$ (fm^4)	$e_{\rm pol}$(IS)	$e_{\rm pol}$(IV)
$1p_{3/2}$	$1p_{3/2}$	3.57	0.423	0.122	3.69	0.418	0.121
$1p_{1/2}$	$1p_{3/2}$	4.17	0.398	0.115	4.35	0.390	0.113
$1d_{5/2}$	$1d_{5/2}$	11.84	0.282	0.081	14.60	0.246	0.071
$2s_{1/2}$	$1d_{5/2}$	15.00	0.132	0.040			

Table 2. Static IS and IV core polarization charges calculated for neutron and proton orbitals in ^{16}C by using SIII force. The neutron $1d_{3/2}$ state is a resonance state in HF potential at $e_{\rm res} = 3.8$ MeV. The real part of the $1d_{3/2}$ wave function is obtained to adjust the box radius of HF calculation in the coordinate space to fit the unbound single-particle energy at the resonance energy. See the text and the captions to table 1 for details.

States		Neutrons			Protons		
f	i	$B(\lambda=2)_{\rm sp}$ (fm^4)	$e_{\rm pol}$(IS)	$e_{\rm pol}$(IV)	$B(\lambda=2)_{\rm sp}$ (fm^4)	$e_{\rm pol}$(IS)	$e_{\rm pol}$(IV)
$1p_{3/2}$	$1p_{3/2}$	4.32	0.299	0.147	4.00	0.315	0.154
$1p_{1/2}$	$1p_{3/2}$	4.75	0.287	0.141	4.29	0.309	0.150
$1d_{5/2}$	$1d_{5/2}$	13.10	0.227	0.104	9.24	0.287	0.130
$2s_{1/2}$	$1d_{5/2}$	15.20	0.133	0.059	7.83	0.230	0.099
$1d_{3/2}$	$1d_{5/2}$	4.79	0.145	0.068	2.89	0.241	0.110
$1d_{3/2}$	$1d_{3/2}$	47.32	0.070	0.035	18.39	0.171	0.079
$2s_{1/2}$	$1d_{3/2}$	41.35	0.067	0.032	15.27	0.161	0.072

where ω_{1^-} is the 1^--phonon energy and c_2 comes from the quadrupole interaction. We should notice that the sign of the particle-vibration matrix element has the opposite sign between the particle and the hole in the same orbit. Therefore the $J = 1/2^+$ state is the lowest in the energy in $^{13}_{8}$O$_5$, while the $J = 3/2^+$ state is the lowest in $^{11}_{3}$Li$_8$. Equations (8) and (9) explain qualitative features of the shell model results in $^{13}_{8}$O$_5$ shown in fig. 1(b). Recently, the Coulomb dissociation cross-sections of $^{13}_{8}$O$_5$ were measured at RIKEN [23]. They claim large $E1$ strength in the same low-energy region as the present calculated results.

3 Quenching of polarization charges and Q-moments of B-isotopes

In order to estimate the polarization due to the core excitations, we use a perturbation with RPA phonons [24, 22,25,16]. The perturbed single-particle wave function is expressed as

$$\mid \tilde{i}\rangle = \mid i\rangle + \sum_{j,\omega_\lambda} \frac{\langle (j\times\omega_\lambda)i \mid V_{\rm pv} \mid i\rangle}{\varepsilon_i - (\varepsilon_j + \omega_\lambda)} \mid (j\times\omega_\lambda)i\rangle\,, \quad (10)$$

where ω_λ represents GR and $V_{\rm pv}$ is the particle-vibration coupling interaction. The reduced transition matrix element for the one-body operator Q^λ is modified as

$$\langle\tilde{j}\|Q^\lambda\|\tilde{i}\rangle = \langle j\|Q^\lambda\|i\rangle + \sum_{\omega_\lambda} \frac{2\omega_\lambda}{(\varepsilon_i-\varepsilon_j)^2 - \omega_\lambda^2} \frac{\sqrt{2i+1}\langle (j\times\omega_\lambda)i \mid V_{\rm pv} \mid i\rangle}{\sqrt{2\lambda+1}} \times \langle\omega_\lambda\|Q^\lambda\|0\rangle. \quad (11)$$

The particle-vibration coupling $V_{\rm pv}$ is derived from the Skyrme interaction . The electric polarization charges for quadrupole moments are defined as

$$e_{\rm pol} = \frac{\langle\tilde{j}\|\, Q^{\lambda=2\,,{\rm el}}\,\|\tilde{i}\rangle}{\langle j\|\, Q^{\lambda=2\,,\tau=0}\,\|i\rangle} - \left(\frac{1}{2} - t_z\right) e\,, \quad (12)$$

where Q^λ expresses one-body operator

$$Q_\mu^{\lambda=2,{\rm el}} = e\sum_{i=1}^{Z} r_i^2 Y_{2\mu}(\hat{r}_i) = \frac{e}{2}\sum_{i=1}^{A}(1-\tau_z) r_i^2 Y_{2\mu}(\hat{r}_i) = \frac{e}{2}(Q_\mu^{\lambda=2,\tau=0} - Q_\mu^{\lambda=2,\tau=1})\,. \quad (13)$$

The IS (IV) polarization charge $e_{\rm pol}^{\rm IS}$ ($e_{\rm pol}^{\rm IV}$) is obtained from the IS (IV) term contribution by $V_{\rm pv}^{\tau=0}$ ($V_{\rm pv}^{\tau=1}$) in the particle-vibration coupling Hamiltonian.

The calculated static polarization charges for ^{12}C core are listed in table 1. Averaged polarization charges for p shell orbits with SIII force are $e_{\rm pol}(n) = 0.53e$ and $e_{\rm pol}(p) = 0.29e$, which are equivalent to the empirical effective charges $e_{\rm eff}(n) = 0.5e$ and $e_{\rm eff}(p) = 1.3e$ commonly used in light nuclei [26]. In tables 2 and 3, the static IS and IV polarization charges calculated with SIII interaction are tabulated for ^{16}C and ^{20}C, respectively.

Table 3. Static IS and IV core polarization charges calculated for neutron and proton orbitals in ^{20}C by using SIII force. The neutron $1d_{3/2}$ state is a resonance state in HF potential at $e_{\rm res} = 3.3$ MeV. See the text and the captions to tables 1 and 2 for details.

States		Neutrons			Protons		
f	i	$B(\lambda{=}2)_{\rm sp}$ (fm^4)	$e_{\rm pol}$(IS)	$e_{\rm pol}$(IV)	$B(\lambda{=}2)_{\rm sp}$ (fm^4)	$e_{\rm pol}$(IS)	$e_{\rm pol}$(IV)
$1p_{3/2}$	$1p_{3/2}$	4.49	0.153	0.132	4.33	0.166	0.141
$1p_{1/2}$	$1p_{3/2}$	4.68	0.149	0.128	4.47	0.165	0.139
$1d_{5/2}$	$1d_{5/2}$	13.37	0.140	0.108	9.04	0.178	0.138
$2s_{1/2}$	$1d_{5/2}$	14.13	0.108	0.078	6.64	0.178	0.127
$1d_{3/2}$	$1d_{5/2}$	4.80	0.087	0.067	2.56	0.168	0.129
$1d_{3/2}$	$1d_{3/2}$	85.59	0.031	0.023	10.97	0.154	0.118
$2s_{1/2}$	$1d_{3/2}$	47.08	0.047	0.034	9.00	0.157	0.112

Table 4. Calculated and experimental Q-moments of B-isotopes. The WBT interaction is used for the shell model calculations, while the core polarization charges are obtained by using SIII interaction. Calculated values $Q^{\rm I}_{\rm cal}$ with the model I are obtained by using the constant effective charges $e_{\rm eff}(n) = 0.5e$ and $e_{\rm eff}(p) = 1.3e$ and harmonic-oscillator wave functions with the oscillator length $b = 1.67$ fm. Calculated values $Q^{\rm II}_{\rm cal}$ with the model II are obtained by using the core polarization charges in table 1 for $A = 10, 11$ and 12, those in table 2 for $A = 13$ and 14 and those in table 3 for $A = 15$ and 17 and HF wave functions of corresponding C-isotopes. The values Q_n and Q_p are obtained with model I and effective charges $e_{\rm eff}(n) = e$ and $e_{\rm eff}(p) = e$. Experimental data are taken from refs. [27,28,13,14]. For details, see the text.

A	J^π	Q_n(mb)	Q_p(mb)	$Q^{\rm I}_{\rm cal}$(mb)	$Q^{\rm II}_{\rm cal}$(mb)	$Q_{\rm exp}$(mb)
10	3^+	44.2	44.2	79.6	82.1	84.72 ± 0.56
11	$\frac{3}{2}^-$	8.75	27.6	40.3	40.3	40.65 ± 0.26
12	1^+	1.14	8.46	11.6	11.3	13.21 ± 0.26
13	$\frac{3}{2}^-$	0.31	30.5	39.8	36.3	36.9 ± 1.0
14	2^-	7.61	16.1	24.7	18.4	29.84 ± 0.75
15	$\frac{3}{2}^-$	44.3	22.9	51.9	37.2	38.01 ± 1.08
17	$\frac{3}{2}^-$	55.8	21.7	56.2	38.9	38.8 ± 1.5

The calculated $e_{\rm pol}$(IS) value decreases rapidly as a function of N/Z to be 0.41, 0.29 and 0.15 for the neutron p shell configurations in ^{12}C, ^{16}C and ^{20}C, respectively. On the other hand, the proton strength below IV GQR remains to be almost the same magnitude in all three isotopes. Thus, the $e_{\rm pol}$(IV) value is rather constant to be $0.12e$ ($0.12e$), $0.14e$ ($0.15e$) and $0.13e$ ($0.14e$) for the neutron (proton) p shell configurations in ^{12}C, ^{16}C and ^{20}C, respectively.

In general, the IS mode is expected to give rise to the IV moment proportional to the neutron excess $(N-Z)/A$ because of the preservation of local ratio of protons to neutrons [22]. This assumption holds approximately in the RPA results in which large IV components are found below the IS GQR peaks in $N > Z$ nuclei [24,16]. Then, the IS contributions to the core polarization charges is expected to have eZ/A-dependence from eq. (13) because of the cancellation between the IS and IV moments in the IS mode. On the other hand, the RPA results show that the IV GQR peaks have very small IS components [16]. This fact suggests that the IV mode keeps the total density unchanged and does not induce the IS moment. Thus, a ratio of electric to the IV quadrupole moment is given as $-e/2$ from eq. (13), which suggests the IV polarization to be rather independent of the N/Z ratio.

We calculate the Q-moments of B-isotopes by using two different models. Firstly, the shell model wave functions are obtained by using the WBT interaction for (p-sd) model space. The $Q^{\rm I}_{\rm cal}$ values with the model I are obtained by using the constant effective charges $e_{\rm eff}(n) = 0.5e$ and $e_{\rm eff}(p) = 1.3e$ and harmonic-oscillator wave functions with the oscillator length $b = 1.67$ fm, for the shell model wave functions. The values $Q^{\rm II}_{\rm cal}$ with the model II are obtained by using the core polarization charges in table 1 for $A = 10, 11$ and 12, those in table 2 for $A = 13$ and 14 and those in table 3 for $A = 15$ and 17, and HF wave functions of corresponding C-isotopes for the same shell model wave functions as the model I. From ^{10}B to ^{13}B, the two models I and II give essentially the same results and show excellent agreement with the experimental data. An important issue drawn by this agreement is that the present particle-vibration model reveals the microscopic origin of the effective charges in stable light nuclei and gives a quantitative justification of the adopted values in the standard shell model calculations. The two results in table 4 deviates slightly in ^{13}B and ^{14}B, and the

conventional model I with the constant effective charges gives few % larger Q-moments than the microscopic model II. The difference between the two calculations becomes larger in ^{15}B and ^{17}B as much as 40%. It is clearly seen in table 4 that the model II results show excellent agreement with the experimental data, but the model I does not. This results justifies a conjecture of the large quenching of the polarization charges in nuclei near drip lines.

4 Summary

We have studied in sect. 2 electric dipole transition strength in the two nuclei with loosely bound nucleons $^{12}_{4}\mathrm{Be}_8$ and $^{13}_{8}\mathrm{O}_5$ by the large-scale shell model calculations including the configuration space up to $3\hbar\omega$ excitations. We found large low-energy $E1$ peaks below 3 MeV in both $^{12}_{4}\mathrm{Be}_8$ and in $^{13}_{8}\mathrm{O}_5$. The calculated results in $^{12}_{4}\mathrm{Be}_8$ show good agreement with the recently observed 1^- state at $E_x = 2.68(3)$ MeV with $B(E1) = 0.051(13)e^2\,\mathrm{fm}^2$ by the Coulomb excitation. We pointed out two key issues to obtain the enhanced $E1$ strength at the low energy. The first one is the effect of the extended wave functions, which enlarges the single-particle transition matrix elements, and also induces the decoupling of the enhanced low-energy $E1$ strength from the GDR strength. The second one is the coherence in the transition amplitudes between the loosely bound nucleons, and also between the core and the loosely bound nucleons. The hole-vibration coupling picture is used to interpret the splittings of both the energies and the strength in $^{13}_{8}\mathrm{O}_5$. In sect. 3, we have studied the N/Z-dependence of the quadrupole polarization charges, using a particle-vibration coupling model together with the HF wave functions and the RPA response functions in ^{12}C, ^{16}C and ^{20}C. We found that both the neutron and proton polarization charges decrease rapidly as a function of N/Z ratio. We applied the obtained polarization charges to calculate the Q-moments of B-isotopes. We found that the present microscopic model gives excellent agreement with the experimental data of all B-isotopes from ^{10}B to ^{17}B, while the conventional model fails to reproduce the experimental Q-moments of ^{15}B and ^{17}B.

This work is supported in part by the Japanese Ministry of Education, Science, Sports and Culture by Grant-In-Aid for Scientific Research under the program number (C(2)) 12640284.

References

1. I. Tanihata *et al.*, Phys. Lett. B **287**, 307 (1992) and references therein; I. Tanihata, J. Phys. G **22**, 157 (1996); P.G. Hansen, A.S. Jensen, B. Jonson, Annu. Rev. Nucl. Part. Sci. **45**, 591 (1995).
2. D.J. Millener *et al.*, Phys. Rev. C **28**, 497 (1983).
3. H. Iwasaki *et al.*, Phys. Lett. B **491**, 8 (2000).
4. H. Sagawa, M. Honma, Phys. Lett. B **251**, 17 (1990).
5. K. Ieki *et al.*, Phys. Rev. Lett. **70**, 730 (1993); D. Sackett *et al.*, Phys. Rev. C **48**, 118 (1993).
6. S. Shimoura, T. Nakamura, M. Ishihara, N. Inabe, T. Kobayashi, T. Kubo, R.H. Siemssen, I. Tanihata, Y. Watanabe, Phys. Lett. B **348**, 29 (1995).
7. M. Zinser *et al.*, Nucl. Phys. A **619**, 151 (1997).
8. T. Nakamura *et al.*, Phys. Lett. B **331**, 296 (1994).
9. A. Navin *et al.*, Phys. Rev. Lett. **85**, 266 (2000).
10. A. Ozawa *et al.*, Phys. Rev. Lett. **84**, 5493 (2000).
11. H. Iwasaki *et al.*, Phys. Lett. B **481**, 7 (2000).
12. K. Asahi *et al.*, *Proceedings RIKEN Symposium on Shell Model 2000, Wako-shi, Japan, March 2000*, to be published in Nucl. Phys. A (2001).
13. K. Izumi, K. Asahi, H. Ueno. H. Okuno, H. Sato, K. Nagata, Y. Hori, M. Adachi, N. Aoki, A. Yoshida, G. Liu, N. Fukunishi, M. Ishihara, Phys. Lett. B **366**, 51 (1996).
14. H. Ogawa *et al.*, *Proceedings RIKEN Symposium on Shell Model 2000, Wako-shi, Japan, March 2000*, to be published in Nucl. Phys. A (2001).
15. I.Hamamoto, H.Sagawa, Phys. Rev. C **54**, 2369 (1996).
16. I. Hamamoto, H. Sagawa, X.Z. Zhang, Nucl. Phys. A **626**, 669 (1997).
17. H. Sagawa, Toshio Suzuki, H. Iwasaki, M. Ishihara, Phys. Rev. C **63**, 034310 (2001).
18. OXBASH, The Oxford, Buenos-Aires, Michigan State, Shell Model Program, B.A. Brown, A. Etchegoyen, W.D. M. Rae, MSU Cyclotron Laboratory Report No. 524 (1986).
19. D.J. Millener, D. Kurath, Nucl. Phys. A **255**, 315 (1975).
20. E.K. Warburton, B.A. Brown, Phys. Rev. C **46**, 923 (1992) and private communications.
21. Toshio Suzuki, H. Sagawa, P.F. Bortignon, Nucl. Phys. A **662**, 282 (2000).
22. A. Bohr, B.R. Mottelson, *Nuclear Structure*, Vol. **II**, edited by W.A. Benjamin (Reading, Massachusetts, 1975).
23. T. Minemura *et al.*, Riken Accelerator Progress Report **33**, 63 (2000).
24. H. Sagawa, K. Asahi, Phys. Rev. C. **63**, 064310 (2001).
25. H. Sagawa, B.A. Brown, Nucl. Phys. A **430**, 84 (1984).
26. B.A. Brown, R. Radhi, B.H. Wildenthal, Phys. Rep. **101**, 313 (1983).
27. P. Raghavan, At. Data Nucl. Data Tables **42**, 189 (1989).
28. T. Minamisono *et al.*, Phys. Rev. Lett. **69**, 2058 (1992).